Stacking-Engineered HfO_2-ZrO_2 Superlattice for Low-Leakage Ferroelectric Memory: First-Principles Design to Device Demonstration

Xiaoyu Dou, Xiaopeng Li, Pengpeng Sang, Xuepeng Zhan, Jixuan Wu, Jiezhi Chen
School of Information Science and Engineering, Shandong University, Qingdao 266237, China
Email: jixuanwu@sdu.edu.cn, chen.jiezhi@sdu.edu.cn

***Abstract*—In this work, we conduct an in-depth study of stacking engineering utilizing HfO_2 and ZrO_2 layers to enhance the performance and reliability of HfO_2-based ferroelectric (FE) devices, achieving significantly reduced leakage current density ($J_{leakage}$). Through first-principles calculation and experimental validation, the $J_{leakage}$-lowering mechanisms in stacking-engineered FE HfO_2-ZrO_2 films are elucidated. Our analysis reveals the phase stability and oxygen vacancy (V_O) formation energy under in-plane tensile strain induced by electrodes. Furthermore, we propose a novel stacking strategy employing superlattice (SL) structures and interface layers (IL) in HfO_2-ZrO_2 films to effectively suppress leakage pathways along grain boundaries and interfaces. Implementing this approach, we achieve a tenfold reduction in leakage current density. This work provides fundamental insights into the physical mechanisms of stacking engineering and offers valuable guidance for process optimization in FE HfO_2-ZrO_2 films.**

Keywords—Ferroelectric (FE), HfO_2-ZrO_2, stacking-structure engineering, leakage current mechanism.

I. Introduction

The discovery of ferroelectricity in HfO_2-based materials attracts paramount interest with their robust ferroelectricity and excellent compatibility with complement-metal-oxide-semiconductor (CMOS) technology [1-2]. These advantages make ferroelectric (FE) HfO_2-based thin films promising candidate for the high-efficiency and low-consumption 3D-integration Non-volatile Memories (NVMs) [3]. But high leakage current density ($J_{leakage}$) induced by high defect concentration, especially oxygen vacancy (V_O), at the interface and grain boundaries limits their scalability and energy efficiency in practical applications [4]. Aiming to address this issue, various engineering strategies are conducted. For example, Wang et al. utilize electrode-oxygen synergy to diminish oxygen vacancy concentration and impede metal diffusion [5]; Tai et al. introduce atom-layer doping to interrupt grain boundaries [6]; and Hsain et al. explore an interfacial engineering strategy to provide excess oxygen [7]. However, these strategies introduce extra elements or complicate the process, hindering their compatibility with 3D integration. In contrast, stacking-engineering strategies, such as the utilization of superlattice (SL) and interface layer (IL), have emerged to improve the leakage-related reliability without complicating the process flow [8-9]. But the underlying physical mechanism remains unclear.

In this work, we investigate the physical mechanism behind stacking engineering in FE HfO_2-ZrO_2 thin films from the aspect of $J_{leakage}$ suppression. First-principles calculations are conducted to analyze the phase stability and V_O defect formation probability in HfO_2 and ZrO_2. The FE orthorhombic phase is found more energetically favorable than that in ZrO_2, while lower formation energy (E_{for}) of V_O reveals higher defect concentration in the Zr rich thin films. Furthermore, the in-plane tensile strain from the electrode mainly applied to the crystal lattice of HfO_2-ZrO_2 thin films during the Rapid Thermal Annealing (RTA) process is considered [9]. After applying strain, E_{for} of V_O in ZrO_2 declines while that remains unchanged in HfO_2, which may deteriorate the $J_{leakage}$ in Zr-dominated regions. Based on the physical insight, we propose three principles for stacking engineering that incorporates both SL and IL using intrinsic HfO_2 and ZrO_2 layers. Experimental verification confirms the feasibility of this approach: $J_{leakage}$ experiences a 90% reduction (4.43×10^{-4} to 4.35×10^{-5}A/cm^2) from the baseline device.

II. First-Principles Calculations

The physical properties of pure-HfO_2, pure-ZrO_2, superlattice HfO_2-ZrO_2, solid-solution (SS) $Hf_{0.5}Zr_{0.5}O_2$ (HZO) and interface are discussed through first-principles calculation. The atomic structures can be referred to our previous work [10]. All simulations are performed with the QuantumATK platform [11]. The Perdew-Burke-Ernzerhof (PBE) generalized gradient approximation (GGA) density functional and SG15 Optimized Norm-Conserving Vanderbilt pseudopotential (ONCVPSP) is used for all calculations.

A. Phase Stability in Slab Model

Since the ferroelectricity of HZO is observed in thin films instead of bulks, surface energy is considered [12]. Following the reported model [13], the slab model is built with 6 unit cells along the polarization direction, and the central 4 unit cells are fixed during the relaxation. In-plane tensile strain is applied directly on the lattice by enlarging lattice constants along A and B axis of (100) plane. Then the surface energy (γ_s) is calculated as the below equation:

$$\gamma_s = (E_{slab} - n\mu_{HfO2}) / 2A \quad (1)$$

here, E_{slab} and μ_{HfO2} are the total energy of the slab and the HfO_2 formula unit of the fully relaxed bulk. n is the number of formulas in the slab structures, and A is the surface area.

As shown in Fig. 1 (a) and (b), AB-biaxial tensile strain reduce the surface energy difference between FE orthorhombic (O) phase and monoclinic (M) phase, while excessively large strain results in a phase transition to the centrosymmetric paraelectric (Para) phase with a space group of *Pbcn*. This phase transition will destroy the ferroelectricity and abnormally increase the surface energy. It's noted that O

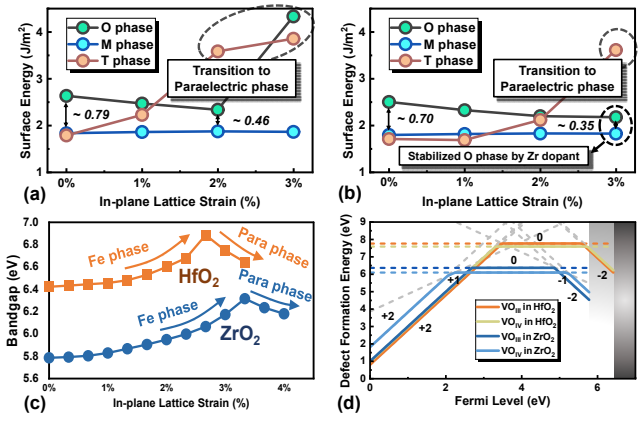

Fig. 1. Surface energy of orthorhombic (O), monoclinic (M) and tetragonal (T) phase under in-plane tensile strain in (a) HfO_2 and (b) ZrO_2. (c) Bandgap of bulk HfO_2 and ZrO_2 accompanied with strain induced Fe-Para phase transition. (d) Defect formation energy of V_O in HfO_2 and ZrO_2. (The grey edges represent different bandgap of these two materials.)

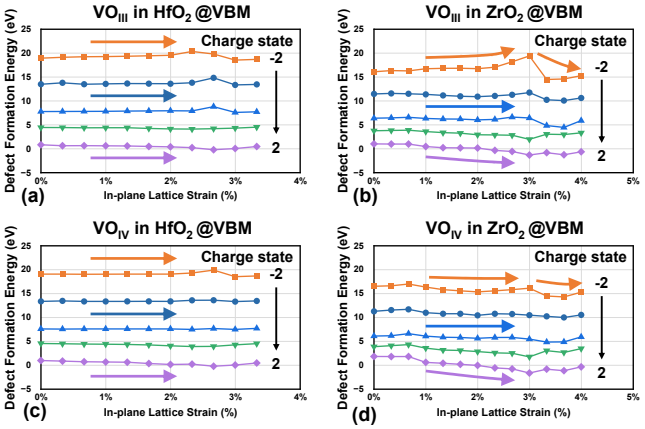

Fig. 2. Formation energy of V_{OIII} and V_{OIV} with charge states from -2 to 2 in (a) and (c): HfO_2; (b) and (d): ZrO_2. The arrows indicate its changing trend when in-plane tensile strain is applied.

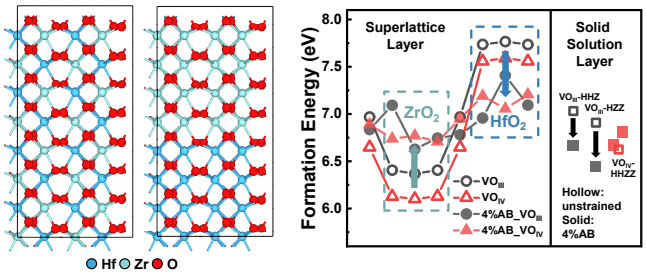

Fig. 3. (a) Atomic structures of SL HfO_2-ZrO_2 (left) and SS (right) HZO. (b) Inhomogeneity distribution of V_O formation energy within SL and SS under unstrained and 4% AB tensile-strain conditions. The blue and grey arrows represent changes of V_O formation energy in HfO_2 and ZrO_2 of SL after applying strain. And the black represents that of SS.

phase is stabilized in ZrO_2 under large strain of 3%, different from the phase transition occurring in HfO_2. This stabilization effect allows a further decline of surface energy from 0.70 to 0.35 J/m^2 in ZrO_2. Moreover, this trend is also demonstrated by the changing of bandgap as illustrated in Fig. 1 (c), which implies detriment to the endurance and breakdown performance as charge injection [14]. As a staged conclusion, Zr dopant is beneficial to O phase crystallization, improving performance of FE devices with HfO_2-based thin films.

B. V_O Formation

The V_O in HZO plays a critical role in the regulation of ferroelectricity consisting remanent polarization (P_r), coercive field (E_c), cycling endurance and leakage current by influencing the crystal phase proportion and pinning the domain walls [15]. Accordingly, the E_{for} of V_O is calculated in the supercell structures of HfO_2, ZrO_2, superlattice HfO_2-ZrO_2 and solid-solution HZO , and the hybrid functional is used to reach a reasonable bandgap. And the E_{for} of a V_O defect in charge state q is expressed as:

$$E_{for} = E_{tot}(q) - E_{tot}(perfect) + \mu_O + q(\varepsilon_F + \varepsilon_{VBM}) + E_{corr} \quad (2)$$

where $E_{tot}(q)$ and $E_{tot}(perfect)$ are total energies of supercells with and without the charged point defect, respectively, and ε_F is the Fermi level energy respect to the valence-band maximum (ε_{VBM}). μ_O is the oxygen chemical potential and E_{corr} is the correction term.

Pure HfO_2 and ZrO_2 show obvious difference in E_{for} of neutral V_O as shown in Fig. 1 (d). It indicates larger V_O concentration in ZrO_2. Furthermore, to examine strain effects, we apply AB-axis tensile strain until 0.67% above the phase transformation strain for HfO_2 (2.67%) and ZrO_2 (3.33%), and evaluate its influence on V_O formation. And exhibited in Fig. 2, downward trend for E_{for} of both three-coordination vacancy (V_{OIII}) and four-coordinate vacancy (V_{OIV}) confirms poorer V_O tolerance of ZrO_2, especially when electrodes which provide large strain are used. This discovery comes to the conclusion that excess Zr ratio may damage the reliability of HfO_2-based FE devices, especially, accelerating the deterioration of $J_{leakage}$.

To mitigate the V_O-induced reliability degradation, superlattice HfO_2-ZrO_2 is proposed previously different from solid-solution HZO [8-9]. Nevertheless, the deep physical mechanisms between superlattice HfO_2-ZrO_2 and solid solution HZO still no clear. Accordingly, the atomic structures of superlattice HfO_2-ZrO_2 and solid-solution HZO are built in this work as shown in Fig. 3 (a). With unstrained condition, different E_{for} (HfO_2 layer > HfO_2/ZrO_2 interface > ZrO_2 layer) in superlattice reveals inhomogeneity distribution of V_O, reducing the growth of leakage paths along grain boundaries and the pinning of domain walls. But in the SS, the E_{for} is lower, making it easier for V_O formation. What's more, after 4% in-plane tensile strain applied, E_{for} in superlattice HfO_2-ZrO_2 converges while it is further decreased in solid solution HZO, emphasizing the advantage of superlattice strategy of $J_{leakage}$ suppressing is addressed.

Based on these findings, three principles are proposed in the stacking engineering to lower $J_{leakage}$ in Zr-doped HfO_2 FE thin films as following:

1) Ensure sufficient Zr content for stabilizing O phase and enhancing P_r;

2) Increase HfO_2-layer thickness to reduce V_O percolation along grain boundaries;

3) Suppress V_O generation at the electrodes/FE interface, especially the bottom electrode (BE) interface degraded by the ALD process [16].

III. Experimental Verification and Discussion

Guided from the above theoretical analysis, 4 kinds of samples with nano-thickness HfO_2-ZrO_2 superlattice and IL are designed for the experimental verification. For comparation and sustain the ferroelectricity, the film thickness is constrained to 10nm (except to sample #4 with 9nm) and the ratio of Hf and Zr is constrained to 1:1.

A. Device Fabrication and Measurement

The key process flow and device structures of FE capacitors are shown in Fig. 4. Firstly, 40nm TiN BE is sputtered on a Si substrate with 300nm SiO_2, followed by HfO_2-ZrO_2 fabrication using ALD at 280°C with superlattice and IL strategy. Then 40nm TiN top electrode (TE) is sputtered and patterned (50μm×50μm) by lithography and lift-off. Lastly, to meet the thermal budget requirements of the back-end-of-line (BEOL) process, 60s RTA is conducted at 400°C in nitrogen atmosphere. The HfO_2-ZrO_2 film of 4 samples are designed as following flow: #1: 10-period (0.5nm HfO_2 / 0.5nm ZrO_2) superlattice; #2: 5-period (1nm HfO_2 / 1nm ZrO_2) superlattice; #3: 1nm HfO_2 (BE IL), 4-period (1nm HfO_2 / 1nm ZrO_2) superlattice, 1nm ZrO_2 (TE IL); #4: 3-period (1.5nm HfO_2 / 1.5nm ZrO_2) superlattice (9nm total). All electrical measurements are executed using Keysight B1500A. The Polarization-Electric field (P-E) loops are measured using positive-up-negative-down (PUND) pulse sweep to avoid the influence of leakage and displacement interference. The frequency of reading and cycling pulse is set to 4kHz.

B. Device Characteristic Analysis

The P-E loops of the four devices at wake-up stage (after 10^5 cycles) are shown in Fig. 5 (a). And Fig. 5 (b) displays the evolution of P_r and E_c during the cycling process extracted from the period of 10^0 to 10^7. During the cycling process, device #3 possesses the largest $2P_{r\_max}$ (27.1μC/cm^2), while device # 4 shows the minimum $2P_{r\_max}$ value of 21.5μC/cm^2. And device #4 exhibits the weakest wake-up effect, with P_r increasing only ~2μC/cm^2 compared to over 6μC/cm^2 in the other devices. Its E_c evolution also remains relatively stable. The suppressed wake-up behavior is consistent with prior work on superlattice structures [8]. Furthermore, it is interesting to find that device #3 exhibits minimal imprint field ($E_{imprint}$~0.06MV/cm @ 10^7 cycles). These discoveries reveal that robust ferroelectricity could be reached in intrinsic HfO_2-ZrO_2 thin films without introducing other doping elements.

As important indexes of device-reliability evaluation, breakdown electric field (E_{BD}) and $J_{leakage}$ are measured, as shown in Fig. 6. Fig. 6 (a) shows the time-zero dielectric breakdown (TZDB) measurements. And the statistics of 15 devices per structure in Fig. 6 (b) reveals that increasing SL thickness significantly improves E_{BD} (17.4% improvement from 3.89MV/cm to 4.57MV/cm). As for the $J_{leakage}$, the measurement is executed under double waveforms of both positive and negative voltage to eliminate polarization-induced current components, as shown in Fig. 6 (c). Then average $J_{leakage}$ of another 15 devices for each structure is extracted at ±3MV/cm and plotted in Fig. 6 (d). The results shows that the $J_{leakage}$ is improve by superlattice stacking in a tenfold reduction (from 4.43×10^{-4}A/cm^2 to 4.35×10^{-5}A/cm^2) at 3MV/cm. Under negative bias, the $J_{leakage}$ is also decreased to about 1/6. It's notable that device #3 shows symmetric $J_{leakage}$ under positive and negative bias, which is attributed to the HfO_2 BE IL.

C. Physical Mechanism

The physical mechanism of the stacking engineering is illustrated in Fig. 7. First, the asymmetry of $J_{leakage}$ derives from more V_O generation at BE/HfO_2-ZrO_2 during the ALD process [16]. When negative voltage is applied, more electron injection induced interface leakage takes place at the BE/HfO_2-ZrO_2 interface due to the V_O trap levels near the

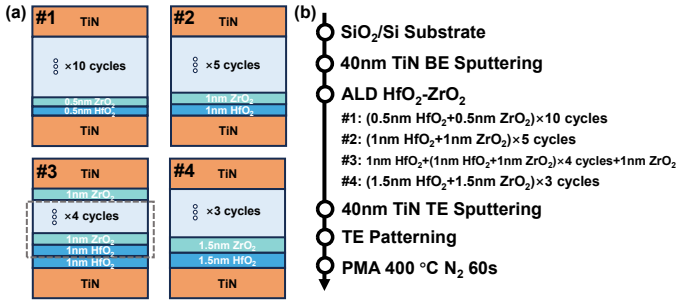

Fig. 4. (a) Device structures and (b) process flow of #1: 0.5nm SL, #2: 1nm SL, #3: 1nm SL with 1nm IL, and #4: 1.5nm SL.

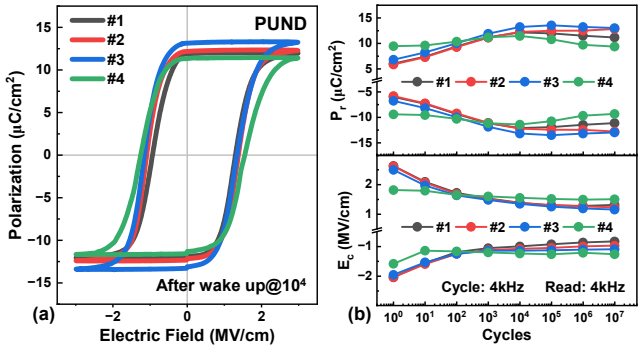

Fig. 5. (a) P-E loops after wake up at 10^5 cycles and (b) endurance measurement of the four FE capacitors.

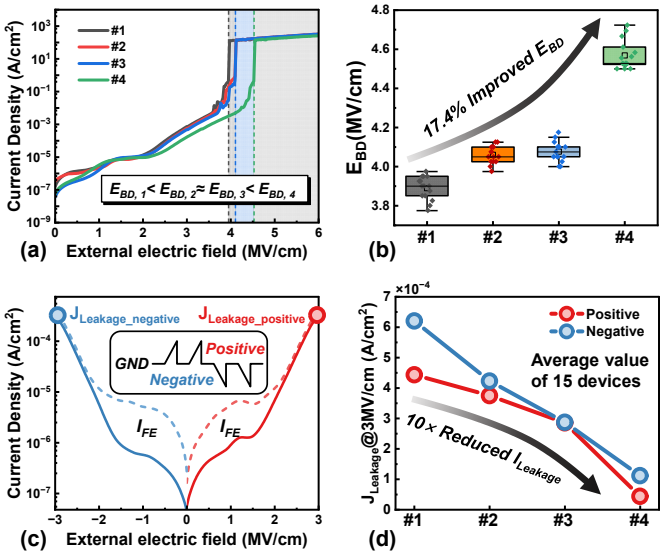

Fig. 6. (a) TZDB measurements of the four devices. (b) Statistics of E_{BD} of 15 devices for each structures. (c) Current-density measurement demonstrated with device #3. The inset shows the measurement strategy of $J_{leakage}$ extracted at ±3MV/cm. (d) Average $J_{leakage}$ of 15 devices for each structure. The arrows represent the changing trend.

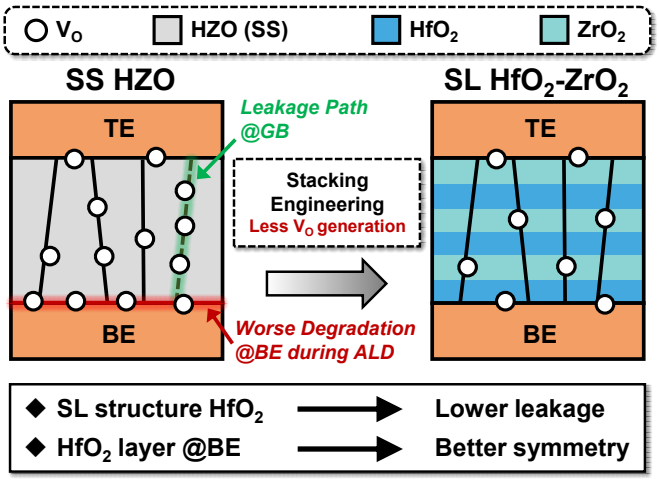

Fig. 7. Schematic of stacking-engineering mechanism by regulating the V_O distribution to reduce the interface and grain-boundary (GB) leakage.

middle of the bandgap as calculated in the Fig. 1 (c). Accordingly, the utilization of BE IL achieves similar $J_{leakage}$ at positive and negative voltage in device #3. Second, in addition to the interface defects, $J_{leakage}$ also originates from the leakage paths along grain boundaries in terms of the previous researches [6]. Thicker superlattice layers suppress the generation of V_O defects within the HfO_2-ZrO_2 thin films by high formation energy of V_O and its inhomogeneity distribution in HfO_2 and ZrO_2 layers. Therefore, the stacking engineering with both superlattice strategy and IL strategy reduces the V_O generation during the process flow and enhances the reliability of intrinsic HfO_2-ZrO_2 thin films.

IV. Conclusions

In this work, we investigate the physical mechanisms underlying stacking-engineered HfO_2-ZrO_2 FE films, achieving significantly reduced $J_{leakage}$. First-principles calculations reveal the phase stability and V_O formation energy in HfO_2 and ZrO_2 under in-plane tensile strain on the (100) plane. Our results demonstrate that ZrO_2 preferentially stabilizes the ferroelectric O phase but simultaneously promotes V_O defect formation under strain. Furthermore, the superlattice structure exhibits an inhomogeneous V_O distribution, suppressing V_O formation more effectively than solid-solution HZO. Guided by these theoretical insights, we propose three design principles for stacking engineering and experimentally validate their efficacy. By introducing a 1nm HfO_2 BE IL, we achieve symmetric leakage current characteristics. Moreover, 1.5nm HfO_2 / 1.5nm ZrO_2 superlattice reduces $J_{leakage}$ by an order of magnitude. Combining first-principles calculation and experimental verification, we elucidate the mechanism by which stacking engineering mitigates leakage—via controlled V_O formation at BE/HfO_2-ZrO_2 interfaces and grain boundaries. These findings provide critical insights for optimizing low-leakage HfO_2-based FE memory devices.

Acknowledgment

This work was supported by China Key Research and Development Program under Grant (2023YFB4402400, 2023YFB4402500), National Natural Science Foundation of China (Nos. U23B2040, 92264201, 62034006, 624B2090), China Postdoctoral Science Foundation (BX20230405), Nationally Funded Postdoctoral Researcher Program (GZC20231435), Natural Science Foundation of Shandong Province (ZR2023QF054), and TaiShan Young Scholars (TSQN202306059).

References

[1] T. S. Böscke, St. Teichert, D. Bräuhaus, J. Müller, U. Schröder, U. Böttger, and T. Mikolajick, "Phase transitions in ferroelectric silicon doped hafnium oxide," Appl. Phys. Lett. 99, 112904 (2011).

[2] J. Müller, T. S. Böscke, S. Müller, E. Yurchuk, P. Polakowski, J. Paul, et al., "Ferroelectric hafnium oxide: A CMOS-compatible and highly scalable approach to future ferroelectric memories," in 2013 IEEE International Electron Devices Meeting (IEDM), pp. 10.8.1-10.8.4.

[3] N. Ramaswamy, A. Calderoni, J. Zahurak, G. Servalli, A. Chavan, S. Chhajed, et al., "NVDRAM: A 32Gb Dual Layer 3D Stacked Non-volatile Ferroelectric Memory with Near-DRAM Performance for Demanding AI Workloads," in 2023 IEEE International Electron Devices Meeting (IEDM), pp. 15.7.1-15.7.4.

[4] X. Li, J. Wu, L. Tai, W. Wei, P. Sang, Y. Feng, et al., "Temperature-dependent Defect Behaviors in Ferroelectric $Hf_{0.5}Zr_{0.5}O_2$ Thin Film: Re-wakeup Phenomenon and Underlying Mechanisms," in 2022 IEEE International Electron Devices Meeting (IEDM), pp. 32.3.1-32.3.4.

[5] X. Wang, M. Wu, T. Zhang, B. Cui, YC. Li, J. Liu, et al., "Exploring tungsten-oxygen vacancy synergy: Impact on leakage characteristics in $Hf_{0.5}Zr_{0.5}O_2$ ferroelectric thin films,". Appl. Phys. Lett. 124, 232901 (2024).

[6] L. Tai, W. Wei, P. Sang, X. Li, X. Dou, G. Zhao, et al., "Silicon Atomic-Layer Doped $Hf_{0.7}Zr_{0.3}O_2$ Films: Toward Low Coercive Field (0.64 MV/cm) and High Endurance (>10^{12} Cycles)," IEEE Transactions on Electron Devices, 2024, 71(7): 4403-4406.

[7] HA. Hsain, Y. Lee, S. Lancaster, PD. Lomenzo, B. Xu, T. Mikolajick, et al., "Reduced fatigue and leakage of ferroelectric TiN/$Hf_{0.5}Zr_{0.5}O_2$/TiN capacitors by thin alumina interlayers at the top or bottom interface," Nanotechnology, 2023, 34(12): 125703.

[8] Y. Peng, W. Xiao, Y. Liu, C. Jin, X. Deng, Y. Zhang, et al., "HfO_2-ZrO_2 Superlattice Ferroelectric Capacitor With Improved Endurance Performance and Higher Fatigue Recovery Capability," IEEE Electron Device Letters, 2022, 43(2): 216-219.

[9] B. Cui, S. Ye, X. Wang, M. Wu, Y. Li, Y. Wu, et al., "Unveiling the Role of Local Stress in Enhancing Ferroelectric Properties and Endurance of HfO_2/ZrO_2 Superlattice Structures," IEEE Electron Device Letters, 2025, 46(1): 107-110.

[10] X. Dou, W. Wei, P. Sang, L. Tai, X. Li, X. Zhan, et at., "Polarization switching pathways of ferroelectric Zr-doped HfO_2 based on the first-principles calculation," Appl. Phys. Lett. 124, 092901 (2024).

[11] S. Smidstrup, T. Markussen, P. Vancraeyveld, J. Wellendorff, J. Schneider, T. Gunst, et al., "QuantumATK: An integrated platform of electronic and atomic-scale modelling tools," J. Phys.: Condens. Matter. 2020, 32, 015901.

[12] MH. Park, YH. Lee, HJ. Kim, T. Schenk, W. Lee, KD. Kim, et al., "Surface and grain boundary energy as the key enabler of ferroelectricity in nanoscale hafnia-zirconia: a comparison of model and experiment," Nanoscale 9(28), 9973–9986 (2017).

[13] J. Wu, F. Mo, T. Saraya, T. Hiramoto, and M. Kobayashi, "A first-principles study on ferroelectric phase formation of Si-doped HfO_2 through nucleation and phase transition in thermal process," Appl. Phys. Lett. 117, 252904 (2020).

[14] J. Huang, GQ. Mao, KH. Xue, S.Yang, F. Ye, H. Sun, X. Miao, "Impact of Zr substitution on the electronic structure of ferroelectric hafnia," J. Appl. Phys. 133, 184101 (2023).

[15] F. Yan, Y. Wu, Y. Liu, P. Ai, S. Liu, S. Deng, et al., " Recent progress on defect-engineering in ferroelectric HfO_2: The next step forward via multiscale structural optimization," Mater. Horiz., 2024, 11, 626.

[16] L. Tai, W. Wei, P. Jiang, P. Sang, X. Li, G. Zhao, et al., "Towards Low-thermal-budget Processing in Ferroelectric $Hf_{0.5}Zr_{0.5}O_2$ Thin Films by Ozone Interface Oxidation," IEEE Electron Device Letters, 2023, 44(12): 1959-1962.